Fast Relaxation on Qutrit Transitions of Nitrogen-Vacancy Centers in Nanodiamonds

A. Gardill◉,[†] M.C. Cambria◉,[†] and S. Kolkowitz◉[*]

Department of Physics, University of Wisconsin, Madison, Wisconsin 53706, USA

Thanks to their versatility, nitrogen-vacancy (N-V) centers in nanodiamonds have been widely adopted as nanoscale sensors. However, their sensitivities are limited by their short coherence times relative to N-Vs in bulk diamond. A more complete understanding of the origins of decoherence in nanodiamonds is critical to improving their performance. Here we present measurements of fast spin relaxation on qutrit transitions between the energy eigenstates composed of the $m_s = |\pm 1\rangle$ states of the N-V^- electronic ground state in approximately 40-nm nanodiamonds under ambient conditions. For frequency splittings between these states of 20 MHz or less the maximum theoretically achievable coherence time of the N-V spin is approximately 2 orders of magnitude shorter than would be expected if the N-V spin is treated as a qubit. We attribute this fast relaxation to electric field noise. We observe a strong falloff of the qutrit relaxation rate with the splitting between the states, suggesting that, whenever possible, measurements with N-Vs in nanodiamonds should be performed at moderate axial magnetic fields (> 60 G). We also observe that the qutrit relaxation rate changes with time. These findings indicate that surface electric field noise is a major source of decoherence for N-Vs in nanodiamonds.

I. INTRODUCTION

Nitrogen-vacancy (N-V) centers in diamond have a number of properties that make them attractive candidates for use as quantum sensors. The N-V^- ground-state electronic spin triplet can be optically polarized and readout via fluorescence, exhibits millisecond-long coherence times at room temperature in bulk diamond [1–4], and can be used as a probe of the local magnetic [5], electric [6,7], strain [8,9], and thermal [10,11] environments. N-Vs in diamond nanocrystals, or nanodiamonds, are particularly attractive for sensing applications as they can be functionalized [12], placed at the ends of scanning tips [5,13], deterministically positioned on nanophotonic structures [14,15], optically levitated [16,17], or even inserted into living cells [10]. Unfortunately, the coherence times of the electronic spins of N-Vs in commercial nanodiamonds are consistently on the order of 1–10 μs [3,18], approximately 2–3 orders of magnitude shorter than what is regularly achieved with N-Vs in bulk diamond [1–4], limiting their sensitivities for many applications. There have been a number of efforts to improve the coherence times of N-Vs in nanodiamonds, including milling from high-purity bulk diamond [19], high-temperature annealing [20], dynamical decoupling [19,21], and a variety of

surface treatments [18,22,23], but thus far only marginal improvements have been observed. A better understanding of the origins of decoherence in nanodiamonds is required to unlock their full potential.

Prior efforts to improve the coherence times of N-Vs in nanodiamonds have focused on magnetic noise as the primary source of both dephasing and relaxation [18,19, 21–23]. However, in a recent work Myers *et al.* found that in shallow N-Vs approximately 7 nm away from the surface in bulk diamond, electric field noise emanating from the surface can drive magnetic-dipole-forbidden transitions with $\Delta m_s = 2$ between the $m_s = |\pm 1\rangle$ states, sometimes called double quantum transitions, at rates up to 2 kHz, or more than 20× the rate between the $m_s = |0\rangle$ state and the $m_s = |\pm 1\rangle$ states [24]. As N-Vs in nanodiamonds are tens of nanometers away from the surface in all directions and the surfaces are more difficult to control than those of bulk diamond samples, it is natural to ask whether this effect occurs in nanodiamonds as well.

Because nanodiamonds frequently exhibit significant intrinsic dc strain or electric fields, it is especially important in this context to distinguish between the eigenstates of S_z and the eigenstates of the N-V spin Hamiltonian. We use $|S_z; m_s\rangle$ to denote the eigenstate of S_z with spin projection m_s. Similarly, we use $|H; m_s\rangle$ to denote the eigenstate of the Hamiltonian with majority component $|S_z; m_s\rangle$. For simplicity, in Figs. 1 and 2 we refer to the state $|H; m_s\rangle$

---

[*]kolkowitz@wisc.edu

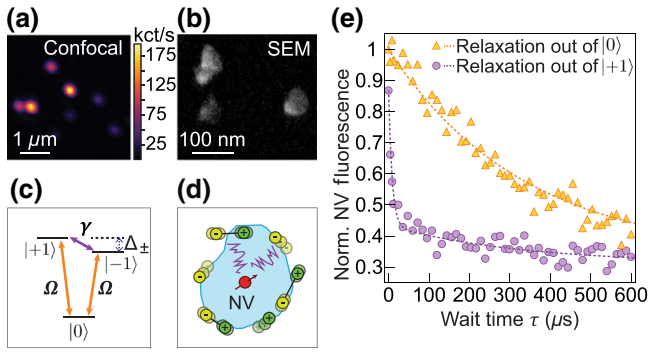[†]These authors contributed equally.

FIG. 1. Fast relaxation on qutrit spin transitions of N-Vs in nanodiamonds. Note that in the figure $|m_s\rangle$ refers to state $|H; m_s\rangle$. (a) Confocal microscope image of N-V centers in nanodiamonds. (b) Scanning-electron-microscope image of three nanodiamonds. (c) Ground-state level structure of the N-V^-. Qubit transitions between $|H; 0\rangle \leftrightarrow |H; \pm1\rangle$ occur at rate Ω, and qutrit transitions between $|H; +1\rangle \leftrightarrow |H; -1\rangle$ at rate γ. (d) Diagram of a single N-V in a nanodiamond. Moving charges or fluctuating electric dipoles create electric field noise (purple lines) that drive N-V spin relaxation. (e) Measurement of state-dependent population relaxation. Relaxation out of $|H; 0\rangle$ (orange triangles) exhibits a single exponential with rate 3Ω. Relaxation out of $|H; +1\rangle$ (purple circles) exhibits a biexponential decay that depends on both Ω and γ (dashed purple line). Dashed lines are Eqs. (1) and (2), and account for π-pulse infidelities, with $\Omega = 1.0$ kHz, $\gamma = 56$ kHz.

as $|m_s\rangle$. We refer to the $|H; -1\rangle \leftrightarrow |H; +1\rangle$ transition as the qutrit transition, a generalization of the $|S_z; -1\rangle \leftrightarrow |S_z; +1\rangle$ double quantum transition [24]. Likewise we refer to the $|H; 0\rangle \leftrightarrow |H; \pm1\rangle$ transitions as the qubit transitions.

In this paper, we present measurements indicating that relaxation on the qutrit transition is a dominant source of decoherence for N-Vs in approximately 40-nm commercial nanodiamonds under ambient environmental conditions. At low axial magnetic fields, $B_z < 10$ G, we find that the rate of relaxation on the qutrit transition can exceed 100 kHz, more than 2 orders of magnitude faster than the rate on the qubit transitions, limiting the maximum theoretically achievable coherence times of N-Vs in this regime to tens of microseconds. We attribute this to electric field noise that drives the transitions between the $|H; \pm1\rangle$ states. We observe this behavior in all five of the single N-Vs in the nanodiamonds that we study. We characterize the dependence of this rate on the frequency splitting, $\Delta_\pm$, between the $|H; \pm1\rangle$ states and observe a strong falloff with $\Delta_\pm$, consistent with a $1/f^2$ scaling of the noise-power spectral density. This indicates that, whenever possible, coherent measurements with nanodiamonds should be performed with moderate magnetic fields (> 60 G) applied along the N-V axis. Finally, we observe fluctuations in this relaxation rate on hour to day timescales, which we consider to be a strong indication that the noise is emanating from the nanodiamond surface.

II. EXPERIMENTAL METHODS

A. Samples and apparatus

All data were taken with commercial nanodiamonds from Adámas Nano, which are crushed from high-pressure high-temperature monocrystalline microdiamonds [25]. Adámas reports that the nanodiamonds have a substitutional nitrogen concentration of approximately 100 ppm before electron irradiation and approximately 60–80 ppm after irradiation and annealing. Adámas annealed the nanodiamonds in vacuum at 850 °C and then oxidized the graphitic layer in acids before suspending the nanodiamonds in solution. The nanodiamond surface is expected to be carboxylated. After receiving the nanodiamond solution, no additional treatment is performed on the nanodiamond surface. Our results are therefore of particular relevance to researchers using similar commercial nanodiamonds without further sample processing. The nanodiamonds have a mean diameter of 40 nm and the diameter distribution has a full width at half maximum of approximately 40 nm. Each nanocrystal contains an average of one–four N-Vs.

The nanodiamonds are diluted in deionized (DI) water to a concentration of 10 μg/ml. To increase the solution's adhesion to the substrate, poly-vinyl alcohol (PVA) is added with a weight-to-weight (PVA to DI water) concentration of 0.17%. A gridded glass coverslip is cleaned with isopropyl alcohol and nanodiamond solution is spin coated onto the coverslip at 3000 revolutions per minute for 20 s. The N-Vs are imaged through the back side of the coverslip, with the nanodiamonds in air under ambient conditions.

Our experimental setup consists of a room-temperature confocal microscope. A fluorescence image of single N-Vs in nanodiamonds is shown in Fig. 1(a), along with a scanning-electron-microscope image of nanodiamonds from the same suspension in Fig. 1(b). Before measuring relaxation rates, we select nanodiamonds containing only single-photon emitters determined by second-order photon-correlation measurements [26]. We then perform optically detected magnetic resonance (ODMR) to select for N-Vs. A majority of the emitters showed low or no contrast ODMR signal. Those N-Vs with a measurable ODMR signal at low magnetic fields were used for experiments (see Table I). In total, we identify five single N-Vs with measurable signals out of a starting set of 110 nanodiamonds.

B. Measurement sequence

As shown in Fig. 1(c), the N-V electronic ground state is a spin triplet. In most N-V studies and applications, a dc magnetic field (B_z) is applied along the N-V axis to lift the degeneracy between the $|H; \pm1\rangle$ states, and the N-V is then treated as a two-level system with a spin
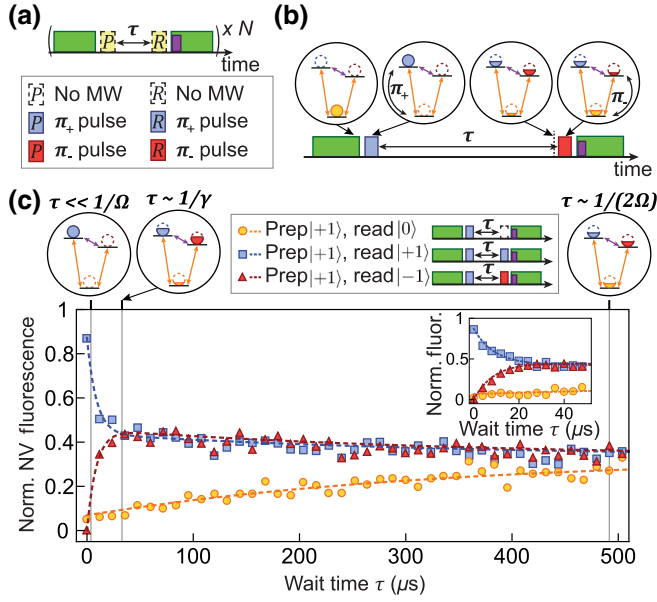
FIG. 2. State-selective population relaxation measurements. Note that in the figure $|m_s\rangle$ refers to state $|H;m_s\rangle$. (a) The measurement sequence consists of preparing N-V in $|H;\pm1\rangle$ or $|H;0\rangle$, waiting time τ, and reading out the population of $|H;\pm1\rangle$ or $|H;0\rangle$. Sequences are repeated $N \sim 10^5$ times. Preparation and readout of population in $|H;0\rangle$ is achieved using 532-nm optical illumination (green rectangles) and fluorescence readout (purple rectangle), while state-selective microwave π-pulses transfer population into and out of $|H;\pm1\rangle$ (red and blue rectangles). (b) Example of single measurement sequence of preparation in $|H;+1\rangle$ and readout in $|H;-1\rangle$. (c) Representative population dynamics for a single N-V in a nanodiamond prepared in $|H;+1\rangle$, with $\Delta_\pm = 28.9(6)$ MHz. The population in states $|H;+1\rangle$ (blue squares), $|H;-1\rangle$ (red triangles), and $|H;0\rangle$ (yellow circles) after wait time τ are measured by the method explained in (a) and (b). Dashed colored lines are solutions to the three-level population-dynamics equations, accounting for π-pulse infidelities, with $\Omega = 1.0$ kHz, $\gamma = 56$ kHz. Inset shows the population dynamics of the same N-V over the first 50 μs of relaxation.

lifetime T_1 found by measuring the lifetime of the $|H;0\rangle$ state. Figure 1(e) shows representative population decay curves for the spin states $|H;0\rangle$ and $|H;+1\rangle$ of an N-V in a nanodiamond. At low B_z, population prepared and

readout in $|H;+1\rangle$ exhibits a biexponential decay and has mostly depolarized after just 20 μs (purple circles). However, the standard T_1 measurement employed in almost all N-V studies, which consists of optically polarizing in $|H;0\rangle$, waiting some time τ, and measuring the population in $|H;0\rangle$ via fluorescence, exhibits a single exponential decay with a much longer time constant of approximately 330 μs (orange triangles). Critically, this measurement is blind to the population leakage between $|H;+1\rangle$ and $|H;-1\rangle$, and would therefore drastically overestimate the achievable coherence time T_2 for this N-V.

Figure 2(a) illustrates the measurement sequence we use to measure the population dynamics into and out of each of the three spin states [24,27,28]. Preparation and readout of any of the three states is achieved by using a combination of 532-nm optical polarization and state-selective resonant microwave π pulses, allowing for a total of nine measurement combinations [26]. For example, Fig. 2(b) shows the sequence used to prepare in $|H;+1\rangle$ and measure the population in $|H;-1\rangle$. After the population is optically polarized into $|H;0\rangle$, a microwave π_+ pulse transfers the population to $|H;+1\rangle$. After a wait time τ, a π_- pulse swaps the populations in $|H;-1\rangle$ and $|H;0\rangle$. The transferred population of the state $|H;-1\rangle$ is then readout out via fluorescence under 532-nm illumination and normalized to a reference measurement of the N-V brightness when it has been polarized in the $|H;0\rangle$ state. The purple circles in Fig. 1(e) correspond to using this sequence to prepare in $|H;+1\rangle$, wait, and then readout in $|H;+1\rangle$.

Figure 2(c) shows a measurement of the population dynamics of the three spin states after preparation in $|H;+1\rangle$ for a representative N-V at a splitting of $\Delta_\pm = 28.9(6)$ MHz. The fast relaxation out of $|H;+1\rangle$ into $|H;-1\rangle$ is readily apparent. Remarkably, the population in $|H;-1\rangle$ is nonmonotonic with time, as the population prepared in $|H;+1\rangle$ first rapidly decays to an even mixture of $|H;\pm1\rangle$ before slowly decaying into an unpolarized mixture of all three spin states.

C. Isolation of rates γ and Ω

To capture the full population dynamics, we solve the rate equations for a generic three-level system with

TABLE I. Characteristics of the five measured N-Vs. For each N-V, the maximum γ we observe is reported with the corresponding splitting $\Delta_\pm^\gamma$, the resulting $T_{2,\text{max}}$, and the contrast of the pulsed ODMR resonance at the splitting $\Delta_\pm^\gamma$. The calculated average Ω_{avg}, γ_∞, and A_0 for each N-V are also listed (see Fig. 3), along with the measured splitting in the absence of any applied magnetic field, $\Delta_\pm^{zf}$. Reported error is twice the standard error.

	Max γ (kHz)	$\Delta_\pm^\gamma$ (MHz)	$T_{2,\text{max}}$ (μs)	ODMR Contrast	Ω_{avg} (kHz)	γ_∞ (kHz)	A_0 (MHz^2 kHz)	$\Delta_\pm^{zf}$ (MHz)
N-V1	117(8)	19.8(6)	16.6(11)	36%	1.1(3)	0.74(6)	33.9(6)$\times10^3$	19.5(6)
N-V2	124(6)	15.3(6)	16.0(8)	40%	0.32(13)	0.20(3)	15.7(2)$\times10^3$	15.3(6)
N-V3	110(20)	17.1(6)	18(3)	20%	1.0(10)	4.7(4)	59(3)$\times10^3$	15.4(6)
N-V4	35(3)	23.4(6)	57(4)	31%	0.30(18)	0.56(4)	29.4(6)$\times10^3$	23.4(6)
N-V5	240(50)	10.9(6)	8.3(17)	10%	0.7(6)	3.7(5)	18.7(18)$\times10^3$	6.9(6)

arbitrary transition rates between each pair of states. Empirically, we find that the transition rates for $|H;0\rangle \leftrightarrow |H;+1\rangle$ and $|H;0\rangle \leftrightarrow |H;-1\rangle$ are equivalent to within our measurement uncertainties [26], which simplifies the analysis. Defining the qutrit transition rate as γ and the qubit transition rate as Ω [see Fig. 1(c)], the population equations for the three N-V states are given by [24,27,29]

$$\rho_0(\tau) = \frac{1}{3} + \left[\rho_0(0) - \frac{1}{3}\right]e^{-3\Omega\tau}, \qquad (1)$$

$$\rho_{\pm 1}(\tau) = \frac{1}{3} \pm \frac{1}{2}\Delta\rho_{\pm 1}(0)e^{-(2\gamma+\Omega)\tau}$$
$$- \frac{1}{2}\left[\rho_0(0) - \frac{1}{3}\right]e^{-3\Omega\tau}, \qquad (2)$$

where τ is the wait time, $\rho_{0,\pm 1}(\tau)$ are the populations of the $|H;0,\pm 1\rangle$ states at time τ, $\rho_0(0)$ is the initial population of $|H;0\rangle$, and $\Delta\rho_{\pm 1}(0)$ is the difference in the initial population of $|H;+1\rangle$ and $|H;-1\rangle$. The dashed colored lines in Figs. 1(e) and 2(c) are plots of Eqs. (1) and (2), accounting for measured π-pulse infidelities [26]. We observe excellent agreement between this model and all of the relaxation measurements we perform.

To extract values for the transition rates γ and Ω, we follow the analysis protocol laid out in Ref. [24]. We denote the time-dependent populations we measure in state $|H;j\rangle$ after initial preparation in $|H;i\rangle$ with $P_{i,j}(\tau)$. From Eqs. (1) and (2), subtracting $P_{0,0}(\tau)$ and $P_{0,+1}(\tau)$ gives

$$F_\Omega(\tau) = P_{0,0}(\tau) - P_{0,+1}(\tau) = ae^{-3\Omega\tau}, \qquad (3)$$

where a is the fluorescence contrast between the two subtracted data sets. Similarly, subtracting $P_{+1,+1}(\tau)$ and $P_{+1,-1}(\tau)$ results in

$$F_\gamma(\tau) = P_{+1,+1}(\tau) - P_{+1,-1}(\tau) = ae^{-(2\gamma+\Omega)\tau}. \qquad (4)$$

This method allows us to fit a single exponential to each subtracted set and isolate the rates Ω and γ. For all five N-Vs we observe $\gamma \gg \Omega$ at low axial magnetic fields. Characteristics of each N-V are summarized in Table I.

III. RESULTS

Figure 3 shows the relaxation rates γ and Ω as a function of the frequency splitting $\Delta_\pm$ for four of the N-Vs measured (similar rates and scalings are also observed for the fifth N-V, see Ref. [26]). The rate γ initially decreases rapidly with increasing $\Delta_\pm$ while Ω appears constant over the measured range $B_z \sim 0 - 200$ G. Similar to the results for shallow N-Vs in bulk diamond [24], the scaling is relatively well described by $\gamma(\Delta_\pm) = A_0/\Delta_\pm^2 + \gamma_\infty$ (dashed purple lines), where A_0 and γ_∞ are constants.

All five of the N-Vs studied here are sampled from a single spin-coated glass coverslip. To verify that the noise
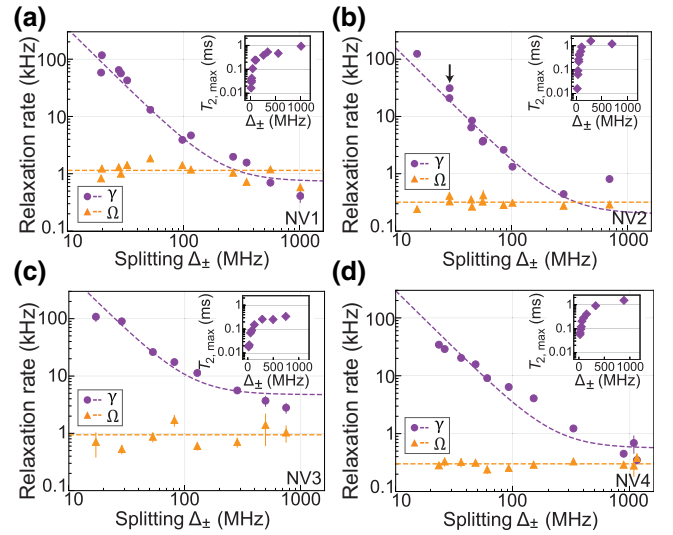

FIG. 3. Dependence of relaxation rates γ and Ω on the frequency splitting between $|H;\pm 1\rangle$ states, $\Delta_\pm$, for four separate N-Vs. Purple circles represent measurement of γ, orange triangles represent measurement of Ω. A fit to $\gamma(\Delta_\pm) = A_0/\Delta_\pm^2 + \gamma_\infty$ is shown on all four plots (dashed purple lines). Error bars are twice the standard error. The point in (b) marked by a black arrow is referenced in Fig. 4. Insets show the corresponding maximum theoretically achievable $T_{2,\max}$ (purple diamonds) based on Eq. (11) on a semilog plot.

we observe is not a result of the glass surface or of the PVA in the solution, we measure a single N-V deposited on a clean silicon wafer from a DI water and nanodiamond solution containing no PVA. The solution is dropped onto a clean silicon wafer and then heated on a hotplate at 160 °C to evaporate the water. We measure the relaxation rates $\gamma = 63(10)$ kHz and $\Omega = 0.17(3)$ kHz of this N-V at splitting $\Delta_\pm = 13.9(6)$ MHz [26]. These rates are similar to the rates measured on the other N-Vs at similar low splittings, confirming the fast-relaxation behavior we observe is intrinsic to the nanodiamonds. Additionally, all measurements are taken with the same power of the 532-nm laser for state polarization and readout. To determine whether this intensity has any effect on the observed rates, we measure γ and Ω of N-V2 at a low splitting at four different laser powers. We find that the rates do not scale with the laser intensity [26].

IV. DISCUSSION

A. N-V Hamiltonian in the nanodiamond context

To discuss the origins of the observed fast transitions between $|H;+1\rangle$ and $|H;-1\rangle$, we introduce the N-V ground-state Hamiltonian. Ignoring hyperfine coupling, the Hamiltonian [30] can be expressed as a sum of the zero-field splitting D_{gs}, the interaction with magnetic field **B**, and the interaction with electric and scaled strain field

Π. That is (with $\hbar = 1$),

$$H = H_{zfs} + H_B + H_\Pi, \qquad (5)$$

where

$$H_{zfs} = D_{gs} S_z^2, \qquad (6)$$

$$H_B = g\mu_B \mathbf{B} \cdot \mathbf{S}, \qquad (7)$$

$$H_\Pi = d_\parallel \Pi_z S_z^2 + d'_\perp \Pi_x (S_x S_z + S_z S_x)$$
$$+ d'_\perp \Pi_y (S_y S_z + S_z S_y) + d_\perp \Pi_x \left(S_y^2 - S_x^2\right)$$
$$+ d_\perp \Pi_y (S_x S_y + S_y S_x). \qquad (8)$$

Here, **S** is the vector of spin-1 operators, $D_{gs}/2\pi = 2.87$ GHz is the zero-field splitting between $|H; 0\rangle$ and $|H; \pm 1\rangle$, $g\mu_B/2\pi = 2.8$ MHz/G is the N-V electronic spin gyromagnetic ratio, and $d_\parallel$, $d_\perp$, and $d'_\perp$ are electric dipole parameters with measured values $d_\parallel/2\pi = 0.35$ Hz cm/V and $d_\perp/2\pi = 17$ Hz cm/V [31]. To our knowledge, $d'_\perp$ has not been measured, but *ab initio* studies suggest $d'_\perp$ and $d_\perp$ may have similar values [30]. However, because the $d'_\perp$ terms mix states with energy splitting approximately D_{gs}, for weak electric fields $d'_\perp$ is frequently taken to be zero [30,31].

In the absence of strain, electric fields, and off-axis magnetic fields, the eigenstates of the Hamiltonian are the same as those of S_z: $|H; m_s\rangle = |S_z; m_s\rangle$. This identification has been made in previous studies of the qutrit transition in shallow N-Vs in bulk diamond [24,28]. In this case, $\langle S_z; -1| H_B |S_z; +1\rangle = 0$, indicating that the $|S_z; -1\rangle \leftrightarrow |S_z; +1\rangle$ qutrit transition is magnetic-dipole-forbidden, while $\langle S_z; -1| H_\Pi |S_z; +1\rangle$ is nonzero. Relaxation on the $|S_z; -1\rangle \leftrightarrow |S_z; +1\rangle$ transition can therefore be unambiguously attributed to resonant electric field and/or strain noise. Because nanodiamonds often contain large intrinsic dc strain or electric fields, the qutrit transition is, in general, not magnetic-dipole-forbidden. Specifically, at zero applied magnetic field the energy eigenstates of N-Vs affected by off-axis strain or electric fields are the bright and dark states $|H; \pm\rangle = \left(|S_z; +1\rangle \mp e^{-i\phi_{\Pi_\perp}} |S_z; -1\rangle\right)/\sqrt{2}$, where $\phi_{\Pi_\perp}$ is the angle of the strain and electric field in the plane transverse to the N-V axis [7]. The $|H; -\rangle \leftrightarrow |H; +\rangle$ transition, like the $|S_z; -1\rangle \leftrightarrow |S_z; +1\rangle$ transition, can be driven by electric field and/or strain noise. Calculation of the $\langle H; -| H_B |H; +\rangle$ matrix element demonstrates that on-axis magnetic noise can also drive the $|H; -\rangle \leftrightarrow |H; +\rangle$ qutrit transition, allowing for the possibility that the fast relaxation rates observed at low applied magnetic field are due to transitions between mixed states driven by magnetic noise. We next investigate this possibility and conclude that it is unlikely.

B. Effect of magnetic field noise on mixed eigenstates

If we treat magnetic field noise as a harmonic perturbation and account for the anisotropy in the effect of the noise by averaging over the possible noise field orientations, then γ_B, the first-order $|H; -1\rangle \leftrightarrow |H; +1\rangle$ relaxation rate due to magnetic field noise, obeys

$$\gamma_B \propto \overline{|\langle H; -1| H_B |H; +1\rangle|^2}, \qquad (9)$$

where H_B is the perturbative magnetic Hamiltonian [Eq. (7)] and $\overline{}$ denotes the average of all possible orientations. Similarly, $\Omega_{B, \pm}$, the first-order $|H; 0\rangle \leftrightarrow |H; \pm 1\rangle$ relaxation rate due to magnetic noise obeys

$$\Omega_{B, \pm} \propto \overline{|\langle H; 0| H_B |H; \pm 1\rangle|^2}. \qquad (10)$$

In order to determine whether the observed $|H; -1\rangle \leftrightarrow |H; +1\rangle$ relaxation is attributable to magnetic field noise or electric field noise, we compare the ratio of Ω and γ where Δ_{0-}, the splitting between $|H; 0\rangle$ and $|H; -1\rangle$, is on the same order of magnitude as $\Delta_\pm$, the splitting between $|H; -1\rangle$ and $|H; +1\rangle$. In this case, we expect that the magnetic noise power at frequency $\Delta_\pm$ is similar in magnitude to the magnetic noise power at frequency Δ_{0-}. We conduct this comparison on N-V1 with $\Delta_{0-} = 2438$ MHz and $\Delta_\pm = 1017$ MHz. This data is marked with an asterisk in Table S1 and shown in Fig. S3 of the Supplemental Material [26]. Using Eqs. (9) and (10) along with numerically calculated eigenstates, we determine the ratio $\Omega_{B, -}/\gamma_B$ to be approximately 25 if we assume that the magnetic noise power is the same at $\Delta_\pm$ and Δ_{0-}. We measure $\Omega = 0.7(2)$ kHz on the $|H; 0\rangle \leftrightarrow |H; -1\rangle$ transition and $\gamma = 0.41(10)$ kHz. The ratio between these two rates is approximately 2, or more than an order of magnitude below what would be expected if magnetic noise were the dominant source of relaxation. This indicates that magnetic noise combined with eigenstate mixing is not a significant source of $|H; -1\rangle \leftrightarrow |H; +1\rangle$ relaxation.

To further test whether or not the fast relaxation we observe is a result of a nonzero γ_B due to eigenstate mixing, we measure γ on N-V1 at a splitting of $\Delta_\pm = 350$ MHz after changing the composition of the eigenstates by rotating the applied magnetic field away from the optimally aligned angle at which the rest of the data for N-V1 is recorded. This data is marked with a dagger in Table S1 of the Supplemental Material [26]. Using Eq. (9) and numerically calculated eigenstates, we can quantitatively describe the ratio of γ_B in the rotated case to γ_B in the aligned case at the same splitting. We calculate this ratio to be approximately 3.5. The measured value of γ in the rotated case is 1.6(2) kHz, whereas the value of γ extrapolated from the empirical fit shown in Fig. 3 in the aligned case is 1.02 kHz. The ratio between these two rates is approximately 1.5, which is comparable to other observed deviations from the fit in Fig. 3. This measured ratio is less than half the

factor of approximately 3.5 that we would expect if the relaxation were dominated by magnetic noise, providing additional evidence that magnetic noise is not the dominant source of qutrit relaxation.

C. Attribution of fast relaxation rates γ to electric field noise

While the numerical analysis described above discounts the possibility that magnetic noise is responsible for the fast qutrit relaxation rates, it does not provide an alternative explanation for our observations. The results of Kim *et al.* [32] and Jamonneau *et al.* [33], whose works analyzed the effect of electric field noise on the coherence times T_2 and T_2^* respectively, suggest that electric field noise is to blame. Importantly, their methodologies are entirely distinct from the qutrit relaxation rate spectroscopy employed here and in Myers *et al.* [24]. Specifically, Kim *et al.* compared the T_2 times of shallow N-Vs before and after applying high dielectric liquid to the bulk diamond surface. Jamonneau *et al.* quantified low-frequency electric field and magnetic field noise by measuring T_2^* for energy eigenstates tuned to be protected against either magnetic field noise or electric field noise. Both groups found evidence of significant low-frequency electric field noise, which supports an interpretation of qutrit relaxation-rate measurements in nanodiamonds as spectroscopic probes of electric field noise, as has previously also been concluded for shallow N-Vs in bulk diamond by Myers *et al.* [24].

Based on the above considerations, we attribute the fast γ relaxation rates to resonant electric field noise at the frequency $\Delta_\pm$ incoherently driving transitions between $|H; \pm 1\rangle$ through the $d_\perp$ terms in Eq. (8) [26]. While our measurements cannot discriminate between strain and electric field noise, based on our observations of the noise changing in time as described below, and guided by other works where electric field noise emanating from surfaces was observed with N-Vs [24,28,32,33] and in other materials systems [34–37], we argue that the observed noise is primarily electric field noise emanating from the nanodiamond surfaces. Under this assumption, the measured relaxation rates are then directly proportional to the perpendicular electric field noise power spectrum: $S_{E_\perp}(\omega) = \gamma(\omega)/(d_\perp^2/h^2)$ [24,28,32]. Using the functions of γ determined in Fig. 3, we integrate $S_{E_\perp}(\omega)$ over the range of measured frequencies $\omega \approx 20 - 1000$ MHz and find an order of magnitude estimate of the root mean square perpendicular component of the electric field $E_\perp^{\mathrm{RMS}} = 10^7$ V/m for all five N-Vs. For comparison, this value is roughly an order of magnitude larger than the dc electric field 20 nm away from a single stationary electron. The $1/f^2$ scaling we observe at lower splittings hints at fluctuating electric dipoles or the motion of charges between charge traps as possible sources of the noise [24]. While our results, in combination with previous studies of the charge noise on

diamond surfaces [24,32,33,38], provide some clues to its origin, the precise nature of the physical process remains an open question. Additionally, we note that Ω_{avg} and γ_∞ are of the same order of magnitude for each of the N-Vs surveyed. This suggests that Ω may also be limited by resonant electric field noise driving $|H; 0\rangle \leftrightarrow |H; \pm 1\rangle$ transitions, and provides indirect evidence that $d_\perp' \neq 0$.

D. Implications for coherence time T_2

Critically, because the relaxation between $|H; \pm 1\rangle$ is an incoherent process, it sets a hard limit on the achievable coherence time T_2 for a N-V spin qubit formed from $|H; 0\rangle$ and either $|H; +1\rangle$ or $|H; -1\rangle$ [24] of

$$T_{2,\mathrm{max}} = 2\,(3\Omega + \gamma)^{-1}. \tag{11}$$

Using the measured values of γ and Ω, this value is plotted as a function of $\Delta_\pm$ in the insets of Fig. 3. At low splitting, $T_{2,\mathrm{max}}$ is severely limited by γ and is approximately 2 orders of magnitude shorter than the erroneous $T_{2,\mathrm{max}}$ that would be calculated under the assumption that the N-V spin is a qubit. These observations may help to explain the mixed results of prior attempts to use dynamical decoupling to extend the coherence times of N-Vs in nanodiamonds [3,19,21]. They also indicate that, whenever possible, measurements with N-Vs in nanodiamonds should be performed at axial magnetic fields exceeding 60 G. In addition, the observed $1/f^2$ noise scaling implies that the electric field noise-power spectral density is even larger at lower frequencies, and as these slowly fluctuating fields shift the energies of the $|H; 0\rangle \leftrightarrow |H; \pm 1\rangle$ transitions through the $d_\parallel \Pi_z S_z^2$ term in Eq. (8), low-frequency charge noise must be considered as a significant source of dephasing in nanodiamonds. This is consistent with the measurements by Jamonneau *et al.* of T_2^* as a function of axial magnetic field performed on a single N-V in a nanodiamond [33].

E. Temporal fluctuations in γ

As shown in Fig. 3, at several values for $\Delta_\pm$ we perform a measurement of γ multiple times and observe deviations well above our standard error. We attribute these deviations to variations in the local electric field noise-power spectral density as a function of time. Figure 4 shows the value of γ as a function of time by performing the same measurement repeatedly on N-V2 at a constant splitting of approximately 29 MHz. The changes in the rate γ in Fig. 4(a) are well outside of the statistical uncertainty of the measurements, and indicate that γ fluctuates in time over hours to days. Similar fluctuations were observed when the same measurements were performed with N-V1 [26], and previously in shallow N-Vs in bulk diamond [24,39]. While the origins of these temporal dynamics are presently obscure, they provide additional evidence that the observed
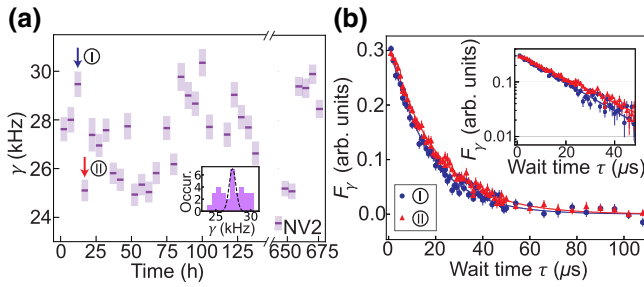
FIG. 4. Temporal fluctuations in the relaxation rate γ. (a) Rate γ of N-V2 at a single splitting $\Delta_{\pm} \approx 29$ MHz (referenced by a black arrow in Fig. 3b) measured for 140 consecutive hours, followed by a 3-week-long gap, then measured again for 35 consecutive hours. Error bars are one standard error. Inset shows a histogram of the measured rates overlaid with a Gaussian curve with standard deviation equal to the average standard error of the measurements. (b) Measured relaxation curves $F_{\gamma}(\tau)$ (Eq. 4) for the back-to-back measurements labeled in (a), illustrating a change in γ that was well above our signal-to-noise ratio. The inset shows the first 50 μs of the same data plotted on a semilog scale. Error bars are one standard error.

noise is primarily from the nanodimaond surfaces, where adsorbates may be coming and going with time.

V. CONCLUSIONS

In conclusion, we present observations of fast relaxation rates on qutrit transitions of N-V electronic spins in nanodiamonds. We find that this relaxation rate depends on the splitting of the $|H; \pm 1\rangle$ levels, and that the resulting limit on the coherence time T_2 improves with higher axial magnetic fields. Additionally, we observe this rate changing with time. Our results demonstrate that the qutrit relaxation rate γ between the $|H; \pm 1\rangle$ states is a critical figure of merit for the coherence of N-Vs in nanodiamonds, and suggest that electric field noise is a major source of both dephasing and relaxation. Beyond the scope of this work, future experiments could be performed to shed light on the origins of this noise and to develop methods for mitigating it, including studies of how γ changes with surface functionalization, nanodiamond size, immersion in dielectric liquids, or temperature. Additionally, measurements of γ could also be used as a local probe of the electric field noise near surfaces in quantum systems limited by charge noise, such as ion traps [35], semiconductor quantum dots [37], and superconducting qubits [34,36].

ACKNOWLEDGMENTS

[1] G. Balasubramanian, P. Neumann, D. Twitchen, M. Markham, R. Kolesov, N. Mizuochi, J. Isoya, J. Achard, J. Beck, and J. Tissler, *et al.*, Ultralong spin coherence time in isotopically engineered diamond, Nat. Mater. **8**, 383 (2009).

[2] G. De Lange, Z. Wang, D. Riste, V. Dobrovitski, and R. Hanson, Universal dynamical decoupling of a single solid-state spin from a spin bath, Science **330**, 60 (2010).

[3] B. Naydenov, F. Dolde, L. T. Hall, C. Shin, H. Fedder, L. C. L. Hollenberg, F. Jelezko, and J. Wrachtrup, Dynamical decoupling of a single-electron spin at room temperature, Phys. Rev. B **83**, 081201 (2011).

[4] N. Bar-Gill, L. Pham, A. Jarmola, D. Budker, and R. Walsworth, Solid-state electronic spin coherence time approaching one second, Nat. Commun. **4**, 1743 (2013).

[5] L. Rondin, J.-P. Tetienne, T. Hingant, J.-F. Roch, P. Maletinsky, and V. Jacques, Magnetometry with nitrogen-vacancy defects in diamond, Rep. Prog. Phys. **77**, 056503 (2014).

[6] F. Dolde, H. Fedder, M. W. Doherty, T. Nöbauer, F. Rempp, G. Balasubramanian, T. Wolf, F. Reinhard, L. C. L. Hollenberg, F. Jelezko, and J. Wrachtrup, Electric-field sensing using single diamond spins, Nat. Phys. **7**, 459 (2011).

[7] T. Mittiga, S. Hsieh, C. Zu, B. Kobrin, F. Machado, P. Bhattacharyya, N. Z. Rui, A. Jarmola, S. Choi, D. Budker, and N. Y. Yao, Imaging the Local Charge Environment of Nitrogen-Vacancy Centers in Diamond, Phys. Rev. Lett. **121**, 6 (2018).

[8] P. Ovartchaiyapong, K. W. Lee, B. A. Myers, and A. C. B. Jayich, Dynamic strain-mediated coupling of a single diamond spin to a mechanical resonator, Nat. Commun. **5**, 4429 (2014).

[9] J. Teissier, A. Barfuss, P. Appel, E. Neu, and P. Maletinsky, Strain Coupling of a Nitrogen-Vacancy Center Spin to a Diamond Mechanical Oscillator, Phys. Rev. Lett. **113**, 020503 (2014).

[10] G. Kucsko, P. C. Maurer, N. Y. Yao, M. Kubo, H. J. Noh, P. K. Lo, H. Park, and M. D. Lukin, Nanometre-scale thermometry in a living cell, Nature (London) **500**, 54 (2013).

[11] D. M. Toyli, C. F. de las Casas, D. J. Christle, V. V. Dobrovitski, and D. D. Awschalom, Fluorescence thermometry enhanced by the quantum coherence of single spins in diamond, Proc. Natl. Acad. Sci. USA **110**, 8417 (2013).

[12] A. Krüger, Y. Liang, G. Jarre, and J. Stegk, Surface functionalisation of detonation diamond suitable for biological applications, J. Mater. Chem. **16**, 2322 (2006).

[13] G. Balasubramanian, I. Chan, R. Kolesov, M. Al-Hmoud, J. Tisler, C. Shin, C. Kim, A. Wojcik, P. R. Hemmer, and A. Krueger, *et al.*, Nanoscale imaging magnetometry with

diamond spins under ambient conditions, Nature (London) **455,** 648 (2008).

[14] S. I. Bogdanov, O. A. Makarova, A. S. Lagutchev, D. Shah, C.-C. Chiang, S. Saha, A. S. Baburin, I. A. Ryzhikov, I. A. Rodionov, A. V. Kildishev, A. Boltasseva, and V. M. Shalaev, Deterministic integration of single nitrogen-vacancy centers into nanopatch antennas, arXiv:1902.05996.

[15] S. Schietinger, M. Barth, T. Aichele, and O. Benson, Plasmon-enhanced single photon emission from a nanoassembled metal-diamond hybrid structure at room temperature, Nano Lett. **9,** 1694 (2009).

[16] L. P. Neukirch, J. Gieseler, R. Quidant, L. Novotny, and A. N. Vamivakas, Observation of nitrogen vacancy photoluminescence from an optically levitated nanodiamond, Opt. Lett. **38,** 2976 (2013).

[17] T. M. Hoang, J. Ahn, J. Bang, and T. Li, Electron spin control of optically levitated nanodiamonds in vacuum, Nat. Commun. **7,** 12250 (2016).

[18] X. Song, J. Zhang, F. Feng, J. Wang, W. Zhang, L. Lou, W. Zhu, and G. Wang, A statistical correlation investigation for the role of surface spins to the spin relaxation of nitrogen vacancy centers, AIP Adv. **4,** 047103 (2014).

[19] H. S. Knowles, D. M. Kara, and M. Atatüre, Observing bulk diamond spin coherence in high-purity nanodiamonds, Nat. Mater. **13,** 21 (2014).

[20] R. Tsukahara, M. Fujiwara, Y. Sera, Y. Nishimura, Y. Sugai, C. Jentgens, Y. Teki, H. Hashimoto, and S. Shikata, Removing non-size-dependent electron spin decoherence of nanodiamond quantum sensors by aerobic oxidation, ACS Appl. Nano Mater. **2,** 3701 (2019).

[21] D.-Q. Liu, G.-Q. Liu, Y.-C. Chang, and X.-Y. Pan, Scaling of dynamical decoupling for a single electron spin in nanodiamonds at room temperature, Physica B **432,** 84 (2014).

[22] F. Brandenburg, R. Nagumo, K. Saichi, K. Tahara, T. Iwasaki, M. Hatano, F. Jelezko, R. Igarashi, and T. Yatsui, Improving the electron spin properties of nitrogen-vacancy centres in nanodiamonds by near-field etching, Sci. Rep. **8,** 15847 (2018).

[23] R. Ryan, A. Stacey, K. M. O'Donnell, T. Ohshima, B. C. Johnson, L. C. L. Hollenberg, P. Mulvaney, and D. A. Simpson, Impact of surface functionalization on the quantum coherence of nitrogen-vacancy centers in nanodiamonds, ACS Appl. Mater. Inter. **10,** 13143 (2018).

[24] B. A. Myers, A. Ariyaratne, and A. C. B. Jayich, Double-Quantum Spin-Relaxation Limits to Coherence of Near-Surface Nitrogen-Vacancy Centers, Phys. Rev. Lett. **118,** 7 (2017).

[25] See the product details from Adámas Nano for more information about these nanodiamonds with item number NDNV40nmLw10ml.

[26] See Supplemental Material at http://link.aps.org/supplemental/10.1103/PhysRevApplied.13.034010 for experimental details and additional data.

[27] S. Kolkowitz, A. Safira, A. A. High, R. C. Devlin, S. Choi, Q. P. Unterreithmeier, D. Patterson, A. S. Zibrov, V. E. Manucharyan, H. Park, and M. D. Lukin, Probing Johnson noise and ballistic transport in normal metals with a single-spin qubit, Science **347,** 1129 (2015).

[28] S. Sangtawesin, B. L. Dwyer, S. Srinivasan, J. J. Allred, L. V. H. Rodgers, K. De Greve, A. Stacey, N. Dontschuk, K. M. O'Donnell, D. Hu, D. A. Evans, C. Jaye, D. A. Fischer, M. L. Markham, D. J. Twitchen, H. Park, M. D. Lukin, and N. P. de Leon, Origins of Diamond Surface Noise Probed by Correlating Single-Spin Measurements with Surface Spectroscopy, Phys. Rev. X **9,** 031052 (2019).

[29] A. Ariyaratne, D. Bluvstein, B. A. Myers, and A. C. B. Jayich, Nanoscale electrical conductivity imaging using a nitrogen-vacancy center in diamond, Nat. Commun. **9,** 2406 (2018).

[30] M. W. Doherty, F. Dolde, H. Fedder, F. Jelezko, J. Wrachtrup, N. B. Manson, and L. C. L. Hollenberg, Theory of the ground-state spin of the NV$^-$ center in diamond, Phys. Rev. B **85,** 205203 (2012).

[31] E. V. Oort and M. Glasbeek, Electric-field-induced modulation of spin echoes of N-V centers in diamond, Chem. Phys. Lett. **168,** 529 (1990).

[32] M. Kim, H. J. Mamin, M. H. Sherwood, K. Ohno, D. D. Awschalom, and D. Rugar, Decoherence of Near-Surface Nitrogen-Vacancy Centers due to Electric Field Noise, Phys. Rev. Lett. **115,** 087602 (2015).

[33] P. Jamonneau, M. Lesik, J. P. Tetienne, I. Alvizu, L. Mayer, A. Dréau, S. Kosen, J.-F. Roch, S. Pezzagna, J. Meijer, T. Teraji, Y. Kubo, P. Bertet, J. R. Maze, and V. Jacques, Competition between electric field and magnetic field noise in the decoherence of a single spin in diamond, Phys. Rev. B **93,** 024305 (2016).

[34] M. H. Devoret, A. Wallraff, and J. M. Martinis, Superconducting qubits: A short review, arXiv:0411174.

[35] M. Brownnutt, M. Kumph, P. Rabl, and R. Blatt, Ion-trap measurements of electric-field noise near surfaces, Rev. Mod. Phys. **87,** 1419 (2015).

[36] B. Christensen, C. Wilen, A. Opremcak, J. Nelson, F. Schlenker, C. Zimonick, L. Faoro, L. Ioffe, Y. Rosen, and J. DuBois, Anomalous charge noise in superconducting qubits, arXiv:1905.13712.

[37] A. V. Kuhlmann, J. Houel, A. Ludwig, L. Greuter, D. Reuter, A. D. Wieck, M. Poggio, and R. J. Warburton, Charge noise and spin noise in a semiconductor quantum device, Nat. Phys. **9,** 570 (2013).

[38] A. Safavi-Naini, P. Rabl, P. F. Weck, and H. R. Sadeghpour, Microscopic model of electric-field-noise heating in ion traps, Phys. Rev. A **84,** 023412 (2011).

[39] D. Bluvstein, Z. Zhang, and A. C. B. Jayich, Identifying and Mitigating Charge Instabilities in Shallow Diamond Nitrogen-Vacancy Centers, Phys. Rev. Lett. **122,** 076101 (2019).